

Structural Characterization and Thermoelectric Transport Properties of Uniform Single-Crystalline Lead Telluride Nanowires

Guo'an Tai, Bin Zhou, and Wanlin Guo*

*Institute of Nanoscience, Nanjing University of Aeronautics and Astronautics,
29 Yudao Street, Nanjing 210016, P.R. China*

Received: May 10, 2008; Revised Manuscript Received: May 28, 2008

Uniform single-crystalline PbTe nanowires with average diameter of about 30 nm, below its average excitonic Bohr radius of 46 nm, were successfully synthesized in large quantity by a two-step hydrothermal process using tellurium nanowires as templates and $\text{Pb}(\text{NO}_3)_2$ as a precursor. It is shown that the reaction temperature, duration, and concentration of $\text{Pb}(\text{NO}_3)_2$ play important roles in the formation of the PbTe nanowires. An in situ diffusion and growth mechanism together with a nontopotactic transformation process was proposed to explain the formation of the PbTe nanowires. The thermoelectric transport measurement indicates a high Seebeck coefficient of about $628 \mu\text{V}/\text{K}$ in the thin film sample composed of the obtained PbTe nanowires, about 137% exceeding that of the state-of-the-art bulk PbTe. The calculated local density of states (LDOS) by the density functional theory shows a strong increase with decreasing nanowire diameter, which is consistent with the measured large enhancement in Seebeck coefficient in the PbTe nanowire sample.

1. Introduction

Thermoelectric materials are important in power generation, cooling and thermal sensing.^{1–6} The performance of thermoelectric devices is quantified by a dimensionless “figure of merit”⁶

$$ZT = T\sigma S^2/k \quad (1)$$

where S , σ , T and k are the Seebeck coefficient, electrical conductivity, absolute temperature, and total thermal conductivity, respectively.⁶ In a bulk material, the Weidmann–Franz law limits the ratio σ/k , which makes optimization of ZT very difficult.¹ In recent years, both theoretical^{7,8} and experimental studies^{9–11} have strongly suggested that large improvements in ZT could be achieved in nanostructured systems. Significant enhancement in thermoelectric conversion efficiency was predicted in quantum-confined systems.^{7,8,12} This enhancement was confirmed recently by the 100-fold improvement in ZT value of silicon nanowires over bulk Si at below or around room temperature, up to $ZT = 0.6–1$.^{13,14}

Lead telluride (PbTe) is particularly promising for high- ZT thermoelectric devices, which is owing to its narrow band gap (0.31 eV at 300 K), face-centered cubic structure and large average excitonic Bohr radius (~ 46 nm) possessing strong quantum confinement within a large range of size.^{11,15} It is reported that PbTe quantum dot superlattices¹¹ and bulk compounds with nanostructures¹⁵ have largely improved energy conversion efficiency compared with their bulk counterparts. Therefore, their synthesis has attracted intensive attentions. Monodispersed PbTe nanocrystals,^{16,17} nanorods,¹⁸ nanoboxes,¹⁹ nanowires,^{20,21} hollow spheres and nanotubes^{22,23} have been synthesized. Theoretical calculations^{8,12} showed that the maximum ZT of one-dimensional (1D) quantum wires is greater than that of the corresponding bulk material. However, to date, the average diameter of the obtained PbTe nanowires is over 60 nm.^{20,21} To improve thermoelectric properties of PbTe remark-

ably, the nanowire diameter of smaller than 46 nm is highly desirable. Moreover, straight nanowires with minimal surface roughness may provide the high carrier mobilities necessary for improving electronic conductivity.²⁴ Additionally, to our knowledge, thermoelectric performance of 1D PbTe nanostructures has not been reported.

Here, a robust two-step hydrothermal synthesis method has been developed to successfully synthesize uniform single-crystalline PbTe nanowires with average diameter of about 30 nm and narrow size distribution in high purity and high yield over 95%. The Seebeck coefficient of the thin film sample composed of the obtained PbTe nanowires exhibits a remarkable enhancement about 137% over that of the state-of-the-art bulk PbTe at room temperature.

2. Experimental Section

2.1. Materials. PVP (polyvinylpyrrolidone, K30, polymerization degree 360, MW = 40 000), sodium tellurite (Na_2TeO_3 , 98%), hydrazine hydrate (85%, w/w%), aqueous ammonia solution (25%, w/w%), and lead nitrate ($\text{Pb}(\text{NO}_3)_2$, 99%) were purchased from Shanghai Chemical Reagent Company.

2.2. Synthetic Procedure of Tellurium Nanowires. Tellurium nanowires are prepared using a modified procedure of the reported method in ref 25. In a typical experiment, polyvinyl pyrrolidone (PVP, 0.30 g) and Na_2TeO_3 (0.1808 g, 0.8mmol) were put into a Teflon-lined stainless steel autoclave (50 mL) and dissolved in double distilled water (25 mL) under vigorous magnetic stirring to form a homogeneous solution at room temperature for several hours. Then hydrazine hydrate (1.5 mL) and aqueous ammonia solution (3 mL) were added into the mixed solution, respectively. The final solution was clear, and double distilled water (10.5 mL) was added into the autoclave under vigorous magnetic stirring. Then the autoclave was closed and maintained at 453 K for 24 h. After that, the container was cooled to room temperature naturally.

2.3. Typical Synthetic Procedure of PbTe Nanowires. $\text{Pb}(\text{NO}_3)_2$ (0.268 g, 0.8mmol) was added into the above solution under magnetic stirring at 278 K for 12 h. Then the autoclave

* Corresponding author. Telephone: +86-25-84895827. Fax: +86-25-84895827. E-mail: wlguo@nuaa.edu.cn.

was closed and maintained at 373 K for 12 h. After the reaction, the black flocculating product was collected from the solution by centrifugation. The precipitates were washed many times with double distilled water and absolute ethanol, and dried in a vacuum at 353 K for 12 h.

2.4. Structural Characterization. The structural properties of the as-prepared products were analyzed by power X-ray diffractometer, which were obtained using Bruker D8 Advance diffractometer with Cu K α radiation ($\lambda=0.154\ 178\ \text{nm}$). The morphology of the as-prepared products was analyzed by field emission scanning electron microscopy (FESEM, Sirion 200, 10 kV). Transmission electron microscopy (TEM), high-resolution TEM (HRTEM), the typical selected area electron diffraction (SAED) patterns and energy dispersive X-ray spectroscopy (EDX) of the nanostructures were performed on JEM-2010 (200 KV).

2.5. Thermoelectric Transport Characterization. In order to measure the electrical conductivity and Seebeck coefficient of the as-synthesized products, a thin film sample was produced by drop-casting the nanowires from dispersed ethanol solutions on a glass substrate. Then the film with length of 25 mm, width of 15 mm and thickness of $26.8\ \mu\text{m}$ was obtained by being pressed using a glass slide after drying naturally in order to make the film more dense and even, then dried at 353 K for 6 h in vacuum. A four-probe method was adopted for the electrical conductivity measurement. Silver pastes dropped in two ends of the thermoelectric film were used as electrical contacts of the electrodes to the sample. The Seebeck coefficient S was measured on a patented thermoelectric measurement instrument (HGTE-II model, national invention 200710051933 of China). The test set up is illustrated in Figure 7c. To decrease the effect of contact resistance on experimental results, a temperature difference of about 9–15 K between cool and hot ends of the film was used for the Seebeck coefficient measurement. The temperature gradient was established in the nanowire film when the electrical power was applied by a thermoelectric pile. The temperature differences (ΔT) were determined by using nickel chromium–nickel silicon thermocouples. The two thermocouples were contacted with the film surface to determine the temperature change. Electrodes pressed on the thermoelectric film were used to monitor the Seebeck voltage drop between the two thermocouples. Seebeck coefficients were determined from the slope of plots of sample voltage versus ΔT .

2.6. Theoretical Calculations. The total density of states calculations were performed using the Vienna ab initio simulation package (VASP) within the density functional theory (DFT) regime.²⁶ To demonstrate the size-dependence of the density of states for each electron, the resulting density of states was obtained by dividing the sum of electrons in each size. In all the calculations, the wave functions were expanded to plane waves with the kinetic energy cutoff of 300 eV and the generalized gradient approximation PBE (Perdew, Burke, and Ernzerhof) was adopted to depict the exchange-correlation energy.²⁷ The PAW pseudopotential was also adopted in our calculations.²⁸ Use these parameters, we relaxed the bulk PbTe with rock salt structure and got the lattice constant is 0.6560 nm, which is larger than the experimental data 0.6454 nm. Then, the nanowires in [100] direction with $1 \times 1 \times 1$, $2 \times 2 \times 1$, $3 \times 3 \times 1$, $4 \times 4 \times 1$ bulk primitive cells as the calculated supercells were established. The diameters of the nanowires are 0.326, 0.992, 1.649 and 2.305 nm, respectively. Periodic boundary conditions were specified in the axial direction. For all nanowire supercells, the 1 nm vacuum layers were used in the two transverse directions to eliminate the interactions of

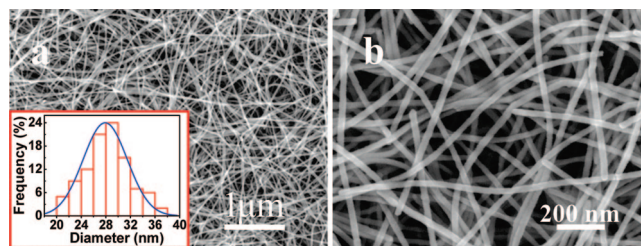


Figure 1. FESEM images of the PbTe nanowires synthesized at 373 K for 12 h: (a) low magnification; (b) high magnification. The inset of part a is the diameter distribution of the nanowires.

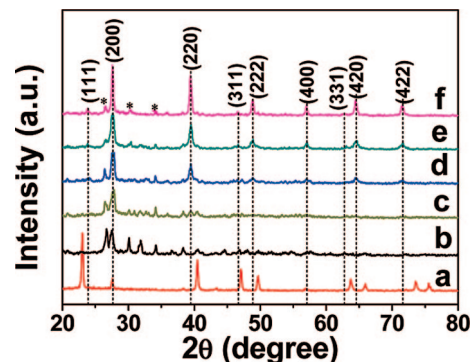


Figure 2. XRD patterns of the Te nanowires (a) and PbTe samples synthesized with different durations: (b) 1, (c) 3, (d) 6, (e) 9 and (f) 12 h. The Miller indices correspond to cubic PbTe crystals. The peaks marked by * are from Pb_3O_4 . The peak positions of the bulk PbTe XRD profile are indicated by short dashed lines for comparison.

the transverse images. The vacuum layer in the transverse direction allows us to simplify the Brillouin zone by only 12 points in the axis direction. The original nanowire models were optimized till the force on each atom was less than 0.001 eV/nm. The optimization do not change the supercell constant for all nanowires.

3. Results and Discussion

3.1. Phase and Morphology Characterization of the PbTe Nanowires. Figure 1 shows the field emission scanning electron microscopy (FESEM) images of the PbTe nanowires with diameter from 20 to 40 nm and length from several to over $100\ \mu\text{m}$. Energy-dispersive X-ray (EDX) spectrum reveals an atomic ratio of $\text{Pb}:\text{Te}=51.15:48.85$ (Figure 3d), close to the stoichiometric PbTe within experimental errors. The signals for Cu, Cr peak were originated from the substrate. The phase of the products was examined by XRD analyses. Figure 2 shows the transformation from tellurium nanowires to PbTe nanowires occurred with increasing reaction durations. The diffraction peaks examined by the XRD pattern (Figure 2f) can be indexed to the purely rocksalt face-centered cubic (fcc) phase of PbTe (space group: $\text{Fm}\overline{3}m$, No.225) with lattice constants of $a = b = c = 0.646\ \text{nm}$ (JCPDS card: 78–1905). The XRD peak positions of the bulk PbTe are indicated by the short dashed lines in Figure 2. The peaks marked “*” are from Pb_3O_4 , which is resulted from a small quantity of nanoplates produced in the product. The reason is that a little oxygen dissolved in the solution can oxidize Pb into PbO_2 in the reaction system, and then the PbO_2 can transform into Pb_3O_4 in the hydrothermal process.²⁹

TEM and HRTEM provide further insight into the details of the obtained nanowires (Figure 3). The SAED (the right inset of Figure 3b) obtained from the individual nanowire shows that the nanowires are single crystalline. And the diffraction spots

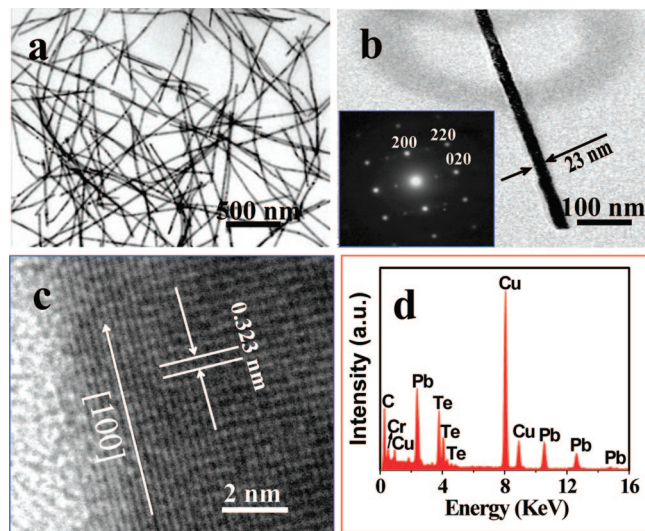


Figure 3. (a) TEM image of PbTe nanowires synthesized at 373 K for 12 h. (b) TEM image of a single nanowire with a diameter of about 23 nm. The inset shows a corresponding SAED pattern of the nanowire taken from the [100] zone axis indicating that the nanowires grow in the $\langle 100 \rangle$ direction. (c) A typical high-resolution TEM image taken from (b). (d) EDX pattern of the nanowires taken from the TEM. The signals for Cu, Cr peaks are originated from the substrate.

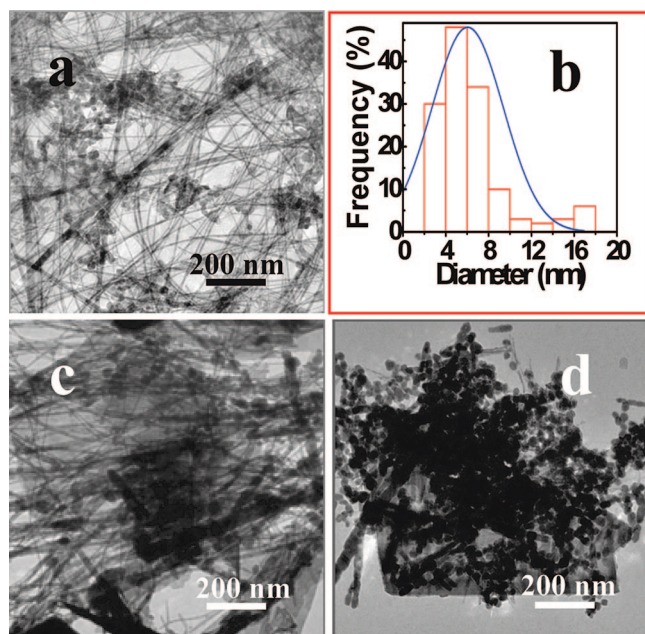


Figure 4. TEM images of the as-synthesized tellurium nanowires (a) and the corresponding diameter distribution (b). The TEM images of the product aged for over 12 h at room temperature (c) and the product prepared for 12 h at 413 K (d).

can be indexed as a cubic, room temperature phase of PbTe. In addition, the HRTEM study (the left inset of Figure 3c) shows that the nanowires are highly crystalline and that the d spacing is 0.323 nm, consistent with the $d(200)$ planes of the fcc PbTe lattice. This value corresponds exactly to the strongest peak observed in the XRD pattern (Figure 2f). Therefore, the nanowires grow along the $\langle 100 \rangle$ direction. The transformed nanowires are thicker than the original Te nanowires. Before the transformation reaction, the Te nanowires are 3~20 nm (Figure 4b) in the diameter. After the reaction, the diameters increase to 20~40 nm (the inset of Figure 1a).

3.2. Investigation of the Growth Mechanism. To understand the growth process of the PbTe nanowires, the effects of

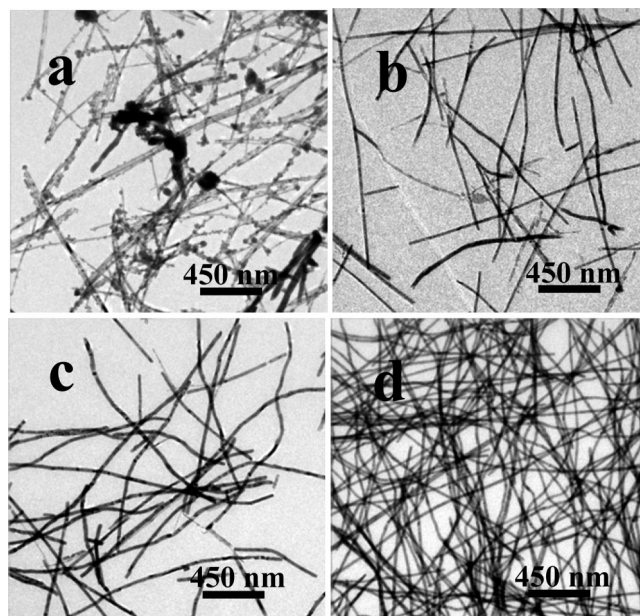
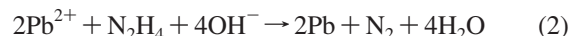


Figure 5. TEM images of the as-synthesized samples at different time intervals: (a) 1, (b) 3, (c) 6, and (d) 9 h.

the reaction temperature, duration, and concentration of $\text{Pb}(\text{NO}_3)_2$ on the resulting products were systematically investigated (Figures 4 and 5). When aged at room temperature over 12 h, a mixture of nanoplates and nanowires was formed (Figure 4c). Further increasing the reaction temperature to 413 K led to produce a mixture of the nanoparticles and nanoplates (Figure 4d). When the rest conditions remained the same, the obtained product was a mixture of nanoparticles and nanowires within 1 h at 373 K (Figure 5a). Prolonging reaction duration to 3 h, the pure nanowires were produced but the nanowires were nonuniform (Figure 5b). Increasing the duration over 9 h, nearly uniform PbTe nanowires were produced (Figure 5c). Well-defined and uniform nanowires of PbTe were obtained when prolonging reaction duration up to 12 h (Figure 1). When the molar ratio of $\text{Pb}(\text{NO}_3)_2$:Te was up to 5, the obtained products were composed of microplates (not shown).

An in situ diffusion and growth mechanism can be proposed to reasonably explain the formation of uniform single-crystalline PbTe nanowires. In the transformation process from t -Te nanowires to PbTe nanowires, the residual hydrazine can reduce Pb^{2+} cations to Pb atoms, which then directly diffuse into the lattice of t -Te to generate cubic PbTe. The net reaction involved in this templating process can be presented as the following:



Because the diffusion coefficient of Pb is greater than that of Te, it is expected that the inward net flow of Pb into the t -Te nanowires can lead to the formation of vacancies in the shell, or the Frenkel disorder.³⁰ The t -Te nanowires can fracture owing to quicker diffusion of Pb than Te atoms at the beginning of the reaction. Simultaneously, PVP as an adsorption agent and architecture soft template plays an important role in the total transformation process. Since PVP can strongly bind metal cations,³¹ it traps the Pb^{2+} that is liberated during the dissolving process, and results in the formation of micelles with Pb^{2+} -polychelate cores.³² Then Pb^{2+} is combined with the t -Te and reduced by the hydrazine in situ near the surface of the template t -Te nanowires (Figure 6a). Thus, Pb atoms can quickly

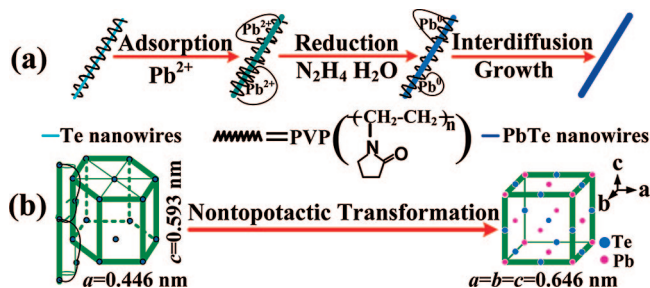


Figure 6. Illustration of the growth mechanism (a) and structural change (b) involved in the transformation from *t*-Te nanowires to PbTe nanowires.

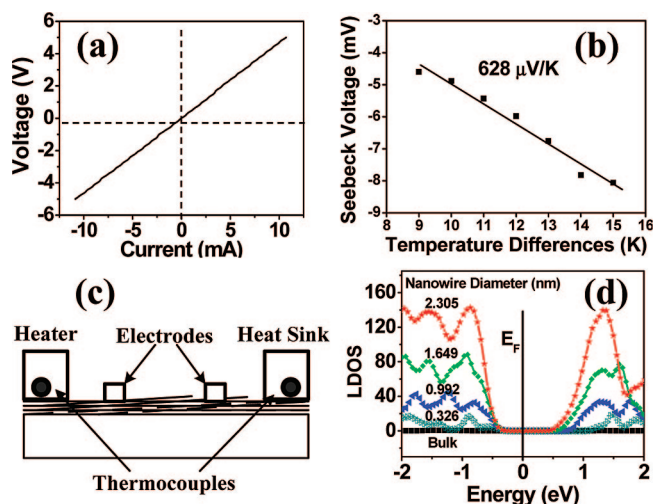


Figure 7. (a) I – V characteristics obtained from a thin film composed of PbTe nanowires. (b) Dependence of the Seebeck voltage as a function of temperature differences along the thermoelectric film. (c) Set up of the measurement configuration for Seebeck coefficient. (d) Local density of states (LDOS) of the different diameter PbTe nanowires and corresponding bulk sample.

diffuse into the *t*-Te nanowires. With increasing reaction duration, the ratio of Pb:Te is close to the stoichiometric composition of PbTe (Figure 1d). In addition, the *t*-Te and PbTe have the hexagonal and cubic structures, respectively (Figure 6b). And they are nontopological in the lattice structure. To our knowledge, this is the first time to synthesize a single-crystal compound nanostructure by a nontopotactic transformation process between the crystal structures of the template nanostructure and product.³³

3.3. Thermoelectric Transport Properties of the PbTe Nanowires. To assess thermoelectric properties of the PbTe nanowires, the room-temperature electrical conductivity and Seebeck coefficient of the as-prepared film consisting of randomly aligned nanowires were measured. The film exhibits a linear current–voltage (I – V) curve (see Figure 7a) that is symmetric about the origin, indicating that the contacts are ohmic. The slope yields a resistance of 466 Ω . By using an average film thickness estimated based on cross-sectional SEM images in a one-dimensional (1D) electrical transport model, an electrical conductivity σ of 133.5 $\Omega^{-1} \text{ m}^{-1}$ can be obtained, which is two orders in magnitude lower than the corresponding bulk sample. The Seebeck coefficient of the nanowire film is 628 $\mu\text{V/K}$ (Figure 7b), which is about 137% enhancement over 265 $\mu\text{V/K}$ of the corresponding bulk sample. Qiu, et al.³⁴ showed that the nanostructured Bi_2Se_3 films exhibited a high Seebeck coefficient of $-119 \mu\text{V/K}$ at room temperature, over two times higher than the bulk Bi_2Se_3 crystal. Liufu, et al.³⁵ also found that Bi_2S_3 nanorod thin films showed a high Seebeck coefficient

up to $-1351 \mu\text{V/K}$ at room temperature, four to five times higher than that of the bulk Bi_2S_3 crystal.

To theoretically demonstrate the enhancement in Seebeck coefficient in the PbTe nanowire film sample, the local density of states (LDOS) of nanowires with different diameters was performed using the periodic DFT program Vienna ab initio simulation package (VASP). The nanowires in [100] direction with $1 \times 1 \times 1$, $2 \times 2 \times 1$, $3 \times 3 \times 1$, $4 \times 4 \times 1$ bulk primitive cells as the calculated supercells were established. The diameters of the nanowires are 0.326, 0.992, 1.649 and 2.305 nm, respectively (Figure 7d). The calculated results show the local density of states exhibits strong increases with decreasing nanowire diameter (see Figure 7d), consistent with the prediction by Dresselhaus et al.⁸ This results in a large enhancement of Seebeck coefficient in comparison with the bulk sample due to an increase in the density of states of electrons near the Fermi level in the nanowires.^{8,12} Additionally, a remarkable depression of the total thermal conductivity is also responsible for the increasing ZT . Fardy, et al.²¹ revealed that the thermal conductivity of the single PbTe nanowire with the diameter of 180 nm is two to 3 orders of magnitude lower than the corresponding bulk sample. Our nanowires should have more lower thermal conductivity than the corresponding bulk sample owing to smaller diameters.⁸

4. Conclusions

In summary, uniform single-crystalline PbTe nanowires with average diameter around 30 nm, which is below its average excitonic Bohr radius, were successfully synthesized in large quantity by a two-step hydrothermal process. First, tellurium nanowires with diameter in the range 3–20 nm were prepared using polyvinyl pyrrolidone and Na_2TeO_3 by a hydrothermal process. Then the PbTe nanowires with diameter of 20–40 nm were successfully synthesized by a second hydrothermal process using the tellurium nanowires as templates and $\text{Pb}(\text{NO}_3)_2$ as a precursor at a molar ratio of 1:1 at 373 K for 12 h. It is shown that the reaction temperature, duration, and concentration of $\text{Pb}(\text{NO}_3)_2$ play important roles in the formation of the PbTe nanowires. An in situ diffusion and growth mechanism together with a nontopotactic transformation process were proposed to reasonably explain the formation of the PbTe nanowires. Thermoelectric transport measurement on the thin film sample from the PbTe nanowires shows a 137% enhancement in the Seebeck coefficient over the reported value of the bulk material, while the electronic conductivity is lowered over 2 orders of magnitude in the PbTe nanowire sample. The Calculated local density of states (LDOS) by the density functional theory shows strong increases with decreasing nanowire diameter, which supports the large enhancement in Seebeck coefficient in the nanowire sample. Measurement on single PbTe nanowires in the present size should show greater burst in thermoelectric performance.

Acknowledgment. The work is supported by the 973 Program (2007CB936204), NSFC (10732040) and the Ministry of Education (No.705021, IRT0534) of China, Jiangsu Province NSF, and the Doctor Innovation Funds of NUAU (No. BCXJ06-04). We thank Prof. Changfeng Chen for helpful discussions.

References and Notes

- (1) Snyder, G. J.; Toberer, E. S. *Nat. Mater.* **2008**, *7*, 105.
- (2) Dresselhaus, M. S.; Chen, G.; Tang, M. Y.; Yang, R. G.; Lee, H.; Wang, D. Z.; Ren, Z. F.; Fleurial, J. P.; Gogna, P. W. *Adv. Mater.* **2007**, *19*, 1.
- (3) Tritt, T. M.; Subramanian, M. A. *MRS Bull.* **2006**, *31*, 188.

- (4) DiSalvo, F. J. *Science* **1999**, *285*, 703.
- (5) Tritt, T. M. *Science* **1999**, *283*, 804.
- (6) Rowe, D. M., Ed. In *CRC Handbook of Thermoelectrics*; CRC Press: New York, 1995.
- (7) Hicks, L. D.; Dresselhaus, M. S. *Phys. Rev. B* **1993**, *47*, 12727.
- (8) Hicks, L. D.; Dresselhaus, M. S. *Phys. Rev. B* **1993**, *47*, 16631.
- (9) Venhatasubramanian, R.; Siivola, E.; Colpitts, T.; O'Quinn, B. *Nature* **2001**, *413*, 597.
- (10) Harman, T. C.; Taylor, P. J.; Spears, D. L.; Walsh, M. P. *J. Electron. Mater.* **2000**, *29*, L1.
- (11) Harman, T. C.; Taylor, P. J.; Walsh, M. P.; LaForge, B. E. *Science* **2002**, *297*, 2229.
- (12) Heremans, J. P.; Thrush, C. M.; Morelli, D. T.; Wu, M. C. *Phys. Rev. Lett.* **2002**, *88*, 216801.
- (13) Hochbaum, A. I.; Chen, R. K.; Delgado, R. Z.; Liang, W. J.; Garnett, E. C.; Najarian, M.; Majumdar, A.; Yang, P. D. *Nature* **2008**, *451*, 163.
- (14) Boukai, A.; Bunimovich, Y.; Tahir-Kheli, J.; Yu, J. K.; Goddard III, W. A.; Heath, J. R. *Nature* **2008**, *451*, 168.
- (15) Hsu, K. F.; Loo, S.; Guo, F.; Chen, W.; Dyck, J. S.; Uher, C.; Hogan, T.; Polychroniadis, E. K.; Kanatzidis, M. G. *Science* **2004**, *303*, 818.
- (16) Mokari, T.; Zhang, M. J.; Yang, P. D. *J. Am. Chem. Soc.* **2007**, *129*, 9864.
- (17) Urban, J. J.; Talapin, D. V.; Shevchenko, E. V.; Murray, C. B. *J. Am. Chem. Soc.* **2006**, *128*, 3248.
- (18) Qiu, X. F.; Lou, Y. B.; Samia, A. C. S.; Devadoss, A.; Burgess, J. D.; Dayal, S.; Burda, C. *Angew. Chem., Int. Ed.* **2005**, *44*, 5855.
- (19) Wang, W. Z.; Poudel, B.; Wang, D. Z.; Ren, Z. F. *Adv. Mater.* **2005**, *17*, 2110.
- (20) Zhang, L. Z.; Yu, J. C.; Mo, M. S.; Wu, L.; Kwong, K. W.; Li, Q. *Small* **2005**, *1*, 349.
- (21) Fardy, M.; Hochbaum, A. I.; Goldberger, J.; Zhang, M. M.; Yang, P. D. *Adv. Mater.* **2007**, *19*, 3047.
- (22) Tong, H.; Zhu, Y. J.; Yang, L. X.; Li, L.; Zhang, L. *Angew. Chem., Int. Ed.* **2006**, *45*, 7739.
- (23) Zou, G. F.; Liu, Z. P.; Wang, D. B.; Jiang, C. G.; Qian, Y. T. *Eur. J. Inorg. Chem.* **2004**, *22*, 4521.
- (24) Cui, Y.; Zhong, Z.; Wang, D.; Wang, W. U.; Lieber, C. M. *Nano Lett.* **2003**, *3*, 149.
- (25) Qian, H. S.; Yu, S. H.; Gong, J. Y.; Luo, L. B.; Fei, L. F. *Langmuir* **2006**, *22*, 3830.
- (26) (a) Kresse, G.; Hafner, J. *Phys. Rev. B* **1993**, *47*, 558. (b) Kresse, G.; Hafner, J. *Phys. Rev. B* **1994**, *49*, 14251. (c) Kresse, G.; Furthmuller, J. *Phys. Rev. B* **1996**, *54*, 11169.
- (27) Perdew, J. P.; Burke, K.; Ernzerhof, M. *Phys. Rev. Lett.* **1996**, *77*, 3865.
- (28) Kresse, G.; Joubert, D. *Phys. Rev. B* **1999**, *59*, 1758.
- (29) Cao, M. H.; Hu, C. W.; Peng, G.; Qi, Y. J.; Wang, E. B. *J. Am. Chem. Soc.* **2003**, *125*, 4982.
- (30) Boltaks, B. I.; Mokhov, Y. N. *J. Tech. Phys. (Russ.)* **1958**, *28*, 1045.
- (31) Vasquez, Y.; Sra, A. K.; Schaak, R. E. *J. Am. Chem. Soc.* **2005**, *127*, 12504.
- (32) Pastoriza-Santos, I.; Liz-Marzan, L. M. *Langmuir* **2002**, *18*, 2888.
- (33) Jeong, U.; Camargo, P. H. C.; Lee, Y. H.; Xia, Y. N. *J. Mater. Chem.* **2006**, *16*, 3893.
- (34) Qiu, X. F.; Austin, L. N.; Muscarella, P. A.; Dyck, J. S.; Burda, C. *Angew. Chem., Int. Ed.* **2006**, *45*, 5656.
- (35) Liufu, S. C.; Chen, L. D.; Yao, Q.; Wang, C. F. *Appl. Phys. Lett.* **2007**, *90*, 112106.

JP8041318